Highly Efficient Hydrogen Evolution over $Co(OH)_2$ Nanoparticles Modified g-C_3N_4 Co-sensitized by Eosin Y and Rose Bengal under Visible Light Irradiation

Zhen Li[a,b], Yuqi Wu[a], Gongxuan Lu[a*]

[a]State Key Laboratory for Oxo Synthesis and Selective Oxidation Lanzhou Institute of Chemical Physics, Chinese Academy of Science, Lanzhou 730000, China.

[b]University of Chinese Academy of Science, Beijing 100049, China.

Abstract

In this work, non-noble metal cobalt hydroxide nanoparticles [$Co(OH)_2$ NPs] implanted uniformly on graphitic carbon nitride (g-C_3N_4) as a co-catalyst for hydrogen evolution reaction (HER) by in-situ chemical deposition method were reported. After co-sensitized by Eosin Y (EY) and Rose Bengal (RB) dyes, this photocatalyst exhibited a comparatively low onset potential (0.26V) for HER and high photocatalytic HER activity under visible light irradiation. The g-C_3N_4 not only provided a large area and nanoporous structure for the confined growth of $Co(OH)_2$ NPs, but also greatly facilitated EY and RB (ER) molecules assembling on its surface, which promoted the charge transfer from dye to co-catalyst. The PL spectra and lifetime test showed the strong interaction between $Co(OH)_2$ NPs and g-C_3N_4 could enhance the transferr rate of the photogenerated electron to reduce the carries recombination. About 431.9 μmol of hydrogen generated over ER co-sensitized $Co(OH)_2$/C_3N_4 in 3 hours. The apparent quantum efficiencies (AQE) of 29.6 and 27.3% were achieved at 530 nm and 560 nm over $Co(OH)_2$/C_3N_4, respectively. In addition, this co-sensitized photocatalyst showed satisfied stability for HER, no remarkable decay of activity was observed in 900 min reaction. These results imply that $Co(OH)_2$ is a stable and efficient cheaper co-catalyst for photo-HER.

Introduction

Photocatalytic water splitting for hydrogen production by sunlight irradiation is one of the most promising routes for the development of clean and renewable energy sources.[1-5] In order to convert solar energy to hydrogen efficiently, a photocatalyst must absorb the most of visible sunlight illumination.[6] g-C_3N_4, a novel and metal-free photocatalyst, has been widely used in water splitting study. Its suitable conduction band position can reduce the H^+ to produce hydrogen from water.[7-9] However, it exhibited pretty low activity under longer wavelength irradiation due to its relatively wide band gap of 2.7 eV.[7] Only shorter than 460 nm light can be absorbed by g-C_3N_4 itself, which leads to wasting about 48% irradiation of sunlight in visible region.

In the past decades, many efforts have been done in improving the visible light response of g-C_3N_4, such as metallic doping,[10-13] nonmetallic doping,[14-18] copolymerization,[19] and integrating g-C_3N_4 with other semiconductors,[20,21] polymer,[22] and electron acceptors (graphene and graphene oxide)[23,24] or introducing mesoporous structure,[25-29] for example, g-C_3N_4 doped with Zn shows an enhanced optical absorption, because of the d-p repulsion of the Zn 3d and N 2p orbitals. Nevertheless, the efficiency for photo-HER was still low under 540 nm irradiation.[13] Doping the g-C_3N_4 with the nonmetallic could modify its electronic properties and extend its optical absorption to the visible region by creating localized/delocalized states in the band gap of g-C_3N_4 matrix, which could efficiently enhance its photocatalytic HER activity. For instance, after partial S substitution of N in g-C_3N_4, the valence bandwidth is increased, which made $C_3N_{4-x}S_x$ photocatalyst workable for photo-HER at 420 nm.[14] Copolymer (g-C_3N_4) obtained by dicyandiamide and barbituric acid could extend its optical absorption up to 750 nm, but the photo-HER activity was still low under irradiation at 460 nm.

For utilizing the full spectrum of solar light efficiently, a strategy of dye sensitization has been applied successfully in dye-sensitized solar cells (DSSCs), and a high photovoltaic conversion efficiency (>15.0%) has been achieved.[6,30] Some pioneer works of dye-sensitized semiconductor for photo-HER gave better light-to-hydrogen energy conversion efficiency,[31] for example, co-sensitized g-C_3N_4

by indole-based LI-4 organic dye and asymmetric ZnPc derivative could absorb the broad visible/NIR light from 400 to 800 nm.[6] The highest AQY (~16.5%) was achieved at 420 nm over Pt/C_3N_4, although its absorptive capacity for visible/NIR light was still relatively weak.

It is known that Pt is an excellent co-catalyst for HER due to its low overpotential, however, high cost precludes widespread use of noble metals.[32-33] Therefore many efforts have been done to search low-cost and high efficient co-catalysts with comparative or even better catalytic activities than Pt. A large amount of studies indicated that Co-based compounds showed high activity for oxygen and hydrogen generation because of its low overpotential. For example, F-doping can enhance the activity of hydrogen generation over Co_3O_4 film by a 5-fold with respect to undoped Co_3O_4.[34] $Co_3(PO_4)_2$ on the inert InO_x electrode also showed low overpotential for oxygen evolution reaction in neutral water.[35] Moreover, Co-based molecular co-catalysts and their derivatives, such as cobaloximes, cobalt porphyrin complexes, diimine-dioxime cobalt compounds and hexaaminocobalt complexes were high-active catalysts for hydrogen and oxygen evolution.[36-41] Their main advantages are as follows: the preparation condition of the hydroxide is more moderate. Hydroxide can combine carrier strongly because its hydroxyl can enhance the electron transfer [42], the charge separation[43] and increase the charge carrier lifetime[44] more efficiently. Metal hydroxide is more favorable to hydrogen production than its oxide due to its low overpotential under the same experimental conditions [45], metal hydroxide could also promote the hydrogen evolution by the pronounced synergetic effect.[46] Therefore metal hydroxide is proposed as potential co-catalyst candidates for HER.

Herein, non-noble cobalt hydroxide NPs implanted on g-C_3N_4 by in-situ chemical deposition methods for high efficient HER were reported. The RB and EY co-sensitized $Co(OH)_2$ NPs exhibited a low onset potential (0.26V) for proton reduction and high HER activities. The g-C_3N_4 provides a large area and nanoporous structure for the confined growth of $Co(OH)_2$ NPs and facilitate ER molecules assembly on its surface, which further improves light harvesting properties. The ER co-sensitization can expand the light absorption range of $Co(OH)_2$/C_3N_4 from 430 nm

to 600 nm. About 432.0 μmol of hydrogen was generated over $Co(OH)_2/C_3N_4$ catalyst in 3 hours under visible light irradiation. The AQEs of 29.6 and 27.3% were achieved at 520 and 550 nm over $Co(OH)_2/C_3N_4$.

Experimental Section

Preparation of the g-C_3N_4 catalysts

Typically, 20 g of urea powder was put into a crucible with a cover and then heated to 600 °C within 30 min in a muffle furnace under the protection of nitrogen and maintained at this temperature for 3 h. The resultant powder was cooled to room temperature, washed with ultrapure water, collected by filtration and finally dried at room temperature.

Photocatalytic hydrogen evolution activity and AQE measurements.

Photocatalytic experiments were performed in a sealed Pyrex flask (150 mL) with a flat window (an efficient irradiation area of 14 cm^2) and a silicone rubber septum for sampling at ambient temperature. In a typical reaction system, 17 mg EY, 25 mg RB, 20mg g-C_3N_4 and 100 μL 1 M $CoCl_2$ aqueous solution were added into 100 ml 10% triethanolamine (TEOA) aqueous solution. The light source was a 300-W Xe lamp and the light density was 100 mW/cm^2, which equipped with either a 420 nm cutoff filter or various band-pass filters. Photon flux of the incident light was determined using a Ray virtual radiation actinometer (FU 100, silicon ray detector, light spectrum, 400-700 nm; sensitivity, 10-50μV$\mu mol^{-1}m^{-2}s^{-1}$). Prior to irradiation, the suspension of the catalysts was dispersed by ultrasonic treatment for 30 min and degassed by bubbling Ar gas for 20 min. The amount of hydrogen evolution was measured using gas chromatography (Aglient 6820, TCD, 13×column, Ar carrier), and the AQE was calculated from the ratio of the number of reacted electrons during hydrogen evolution to the number of incident photons by the following equation:

AQE [%] = 2×number of evolved H_2 molecules / number of incident photos×100

Working Electrode Preparation and Photoelectrochemical Measurements

Photocurrent responses of catalyst samples were measured on an electrochemical analyzer (CHI660E) in a homemade standard three-compartment cell, consisting of an organic glass container with a quartz window and a 1.2cm diameter opening opposite the window to the work electrode was clamped. The working electrodes were prepared by drop-coating sample suspensions directly onto the precleaned indium tin oxide glass (ITO glass) surface by microsyringe with an infrared heat lamp to speed drying. The surface of working electrode exposed to the electrolyte was a circular film with the geometrical surface areas of 1 cm^2. Platinum foil was used as a counter electrode and a saturated calomel electrode (SCE) was used as the reference electrode. The supporting electrolyte was 10% TEOA aqueous solution mixed with 0.1 M Na_2SO_4 aqueous solution. A 300-W Xe lamp with an optical cutoff filter ($\lambda \geq 420$ nm) was used for excitation light source. The unbiased anodic photocurrent was investigated with an amperometric current-time technique.

Characterizations

Transmission electron microscopy (TEM) images were taken with a Tecnai-G2-F30 field emission transmission electron microscope operating at accelerating voltage of 300 kV. The X-ray diffraction patterns (XRD) of the samples were recorded on a Rigaku B/Max-RB X-ray diffractometer with a nickel-filtrated Cu Kα radiation. The accelerating voltage and current were 40 kV and 30 mA, respectively. XPS analysis was performed using a VG ScientificESCALAB210-XPS photoelectron spectrometer with a Mg KRX-ray resource. FT-IR spectra were measured on a Nexus 870 FT-IR spectrometer from KBr pellets as the sample matrix. UV-vis Diffuse Reflectance Spectra were obtained with a Shimadzu UV-3600 UV-vis-near-IR spectrophotometer. $BaSO_4$ was used as a reflectance standard. The fluorescence decay times and photoluminescence (PL) spectra were measured using the Horiba Jobin Yvon Data Station HUB operating in time-correlated single photon counting mode (TCSPC) with the time resolution of 200 ps. Nano LED diode emitting pulse sat 460 nm with 1 MHz repetition rate was used as an excitation source. Light-scattering Ludox solution was used to obtain the instrument response function (prompt). The time ranges are0.055

ns/channel in 4096 effective channels. Horiba Jobin Yvon DAS6 fluorescence decay analysis software was used to fit the model functions to the experimental data.

Results and Discussion

The route of formation of the $Co(OH)_2/C_3N_4$ composite is illustrated in Scheme 1. The g-C_3N_4 suspension was ultrasonicated in a TEOA solution to give a homogeneous g-C_3N_4 dispersion, and then $CoCl_2$ solution was added gradually to the suspension, in which Co^{2+} was first adsorbed on the surface of g-C_3N_4 through coulomb forces because of its negative charge and then reacted with OH^- to form $Co(OH)_2$ NPs, resulting in the $Co(OH)_2/C_3N_4$ composite. The XRD characterization of C_3N_4 was carried out and the result was shown in Fig.1. The strongest diffraction peak at 27.4° (d=0.325) was belonged to the dense interlayer-stacking (002) peak of aromatic segment, as a graphite-like packing characteristic of g-C_3N_4 materials.[25,26] The peak at 13.1° (0.713 nm) was attributed to (100) peak that arose from the in-plane ordering of tri-s-triazine units.[8] In addition, the smaller in-planar distance (d = 0.677 nm) than one tri-s-triazine unit (0.713 nm) was presumably owing to the presence of small tilt angularity in the structure. After implanting Co specie on the surface of C_3N_4, a new peak centered at 44.5° was detected, which could be assigned to (101) facet of $Co(OH)_2$. This result indicates the Co specie existed in the form of $Co(OH)_2$ on the surface of C_3N_4. The average size of $Co(OH)_2$ was about 3.0 nm from the line width analysis of the (101) diffraction peak using Scherer equation.

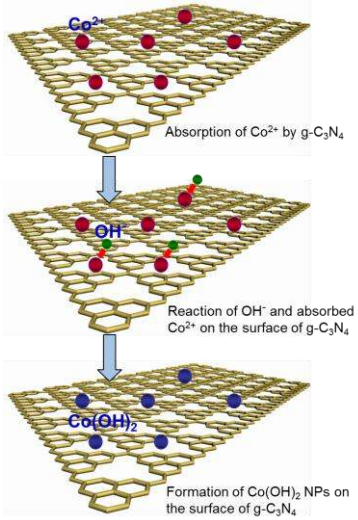

Scheme 1 Formation of $Co(OH)_2/C_3N_4$ by the *in situ* chemical deposition method.

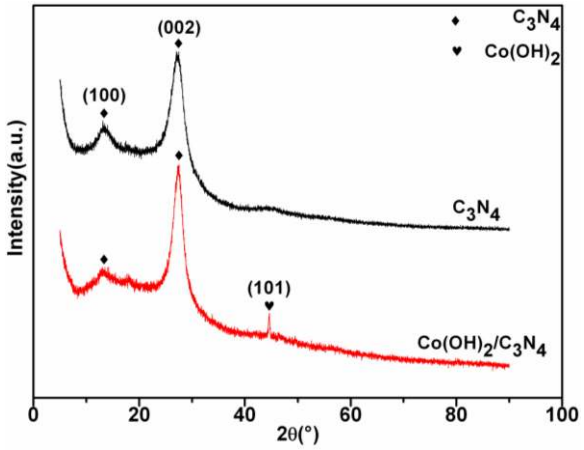

Fig. 1 Experimental XRD patterns for g-C_3N_4 and $Co(OH)_2/C_3N_4$ photocatalysts.

In order to further study the structure and performance of C_3N_4 and $Co(OH)_2/C_3N_4$ catalysts, the FT-IR spectra is carried out and the results were shown in Fig. 2. The peaks at 1200 and 1750 cm^{-1} corresponded to the characteristic stretching modes of C-N heterocycles. The peak at 809 cm^{-1} belonged to the breathing mode of triazine units. The characteristic features of the condensed C−N heterocycles, i.e., the typical breathing mode was centered at 806.5 cm^{-1}. In addition, the peaks at 1315.7 and 1241.2 cm^{-1} corresponded to the stretching vibrations of the connected units of $N-(C)_3$ (full condensation) and C−N−C (partial condensation), respectively. While the peaks at 1645.3, 1564.6, and 1408.2 cm^{-1} represented the stretching vibration modes of heptazine-derived repeating units.[47-50] All these peaks represented typical characteristics of C_3N_4. After loading $Co(OH)_2$ nanoparticles on the surface of C_3N_4, no obvious difference was found, indicating no damage of C_3N_4 structure due to formation of $Co(OH)_2$ nanoparticles.

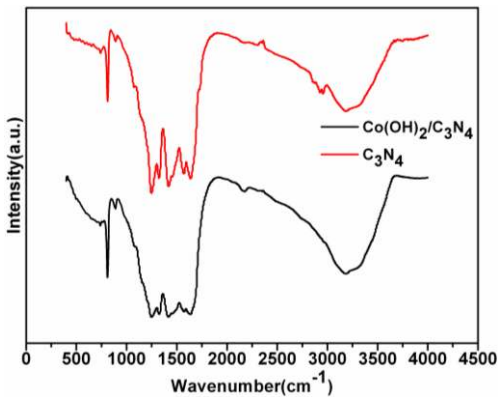

Fig. 2 The FT-IR spectra of C_3N_4 and $Co(OH)_2/C_3N_4$ photocatalysts.

The XPS spectra of C_3N_4 and $Co(OH)_2/C_3N_4$ catalysts were measured to further study the chemical state of C_3N_4 and Co species, and the results were shown in Fig. 3. In the Fig. 3A, the peak of C 1s spectra of g-C_3N_4 centered at 288.3 eV could be attributed to sp2-bonded carbon (N-C=N) species, while the weak one at 286.3 eV could be attributed to sp3-bonded carbon (N-C) species.[51] After loading $Co(OH)_2$ NPs, those binding energy peaks were slightly shifted toward more positive to 288.5 eV and 286.7 eV, respectively. These results indicated there were strong interaction between g-C_3N_4 and $Co(OH)_2$ NPs, which could promote the electron transfer from g-C_3N_4 to $Co(OH)_2$ NPs. Thus interaction was also identified by N 1s spectra as shown in Fig. 3B. The peak centered at 398.8 eV corresponded to sp2 hybridized aromatic N bonded to carbon atoms (C=N-C). The peak centered at 399.8 eV corresponded to the tertiary N bonded to carbon atoms in the form of $N\text{-}(C)_3$ or $H\text{-}N\text{-}(C)_2$.[52] The weaker peak with a high binding energy at 401.3 eV corresponded to quaternary N bonded to three carbon atoms in the aromatic cycles.[50,52] And the peak centered at 404.4eV belonged to the π excitation.[53-54] After loading $Co(OH)_2$ NPs, the peaks also shifted slightly high binding energy to 399.1, 400.5, 401.7 and 404.9 eV, respectively. Upon this interaction, the photogenerated charges might transfer more easily from g-C_3N_4 to $Co(OH)_2$ and reduce the rate of the carries recombination, as a result, the charge lifetime was prolonged and eventually led to the highly efficient hydrogen evolution activity. In Fig. 3c, the peaks centered at 781.1 and 797.0 eV were attributed to Co 2p3/2 and 2p1/2, indicating Co existed in the form of $Co(OH)_2$. These results were in good agreement with the XRD.

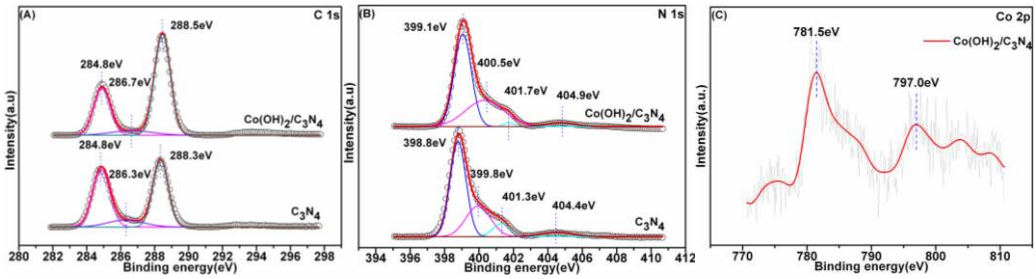

Fig. 3 The XPS spectra of C_3N_4 and $Co(OH)_2/C_3N_4$ photocatalysts. a) C1s specta. b) N1s spectra. c) Co 2p spectrum.

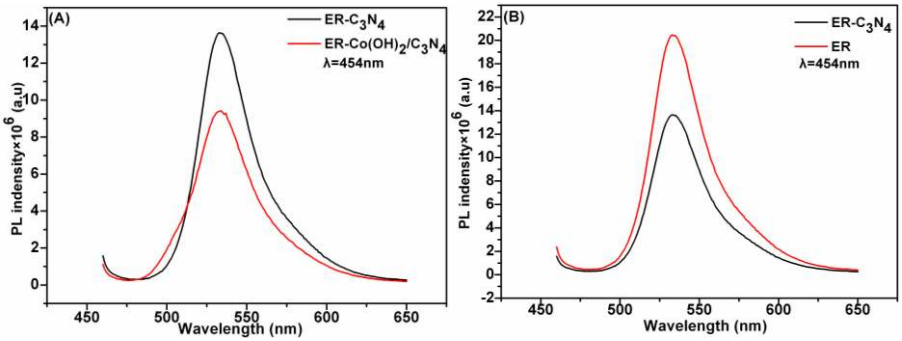

Fig. 4 PL spectra of ER and the quenching effect of addition of g-C_3N_4 and $Co(OH)_2/C_3N_4$.

Table 1 Fluorescence lifetime measurements of EY and/or RB sensitized g-C_3N_4 and $Co(OH)_2/C_3N_4$ catalysts.

C_3N_4 systems	Lifetime, <τ> (ns)	Pre-exponential factors *B*	Average lifetime,<τ> (ns)	χ^2
EY	τ_1=1.21	B_1=1	1.21	0.9999
RB	τ_1=0.43	B_1=1	0.43	1.0037
ER	τ_1=1.02 τ_2=1.67	B_1=0.7356 B_2=0.2644	1.19	1.0048
EY-$Co(OH)_2/C_3N_4$	τ_1=1.65 τ_2=3.41	B_1=0.8105 B_2=0.1895	1.98	0.9992
EY-C_3N_4	τ_1=1.37 τ_2=3.14	B_1=0.8527 B_2=0.1473	1.63	1.0060
RB-$Co(OH)_2/C_3N_4$	τ_1=0.92 τ_2=3.53	B_1=0.5041 B_2=0.4959	2.21	1.0140
RB-C_3N_4	τ_1=0.76 τ_2=3.23	B_1=0.7173 B_2=0.2827	1.46	1.0450
ER-$Co(OH)_2/C_3N_4$	τ_1=0.92 τ_2=1.48 τ_3=3.66	B_1=0.0635 B_2=0.8191 B_3=0.1173	1.70	1.0204
ER-C_3N_4	τ_1=0.78 τ_2=1.31 τ_3=3.11	B_1=0.0782 B_2=0.8007 B_3=0.1211	1.49	1.0462
$Co(OH)_2/C_3N_4$	τ_1=2.98	B_1=1	2.98	1.0864
C_3N_4	τ_1=2.31	B_1=1	2.31	1.0835

The PL spectra further confirmed the promotion of charge separation and prolong of charge lifetime in $Co(OH)_2$ NPs loaded g-C_3N_4 (see results in Fig. 4). The strong PL of ER co-sensitized g-C_3N_4 indicated the fast carrier recombination, and an obvious quenching effect could be observed with the loading of $Co(OH)_2$ NPs, implying that the strong interaction was existed between $Co(OH)_2$ NPs and g-C_3N_4. The PL intensities of ER decreased significantly (see Fig. 4B). These results suggested that photogenerated electron of the excited ER could be efficiently transferred to the conduction band (CB) of g-C_3N_4 because there was no overlap between the absorption bands of ER and g-C_3N_4.[6] The fluorescence lifetime further proved these conclusion (see Table 1). In the EY-C_3N_4, RB-C_3N_4 and ER-C_3N_4 systems, the average lifetime were 1.63, 1.46 and 1.49 ns respectively. However, after loading $Co(OH)_2$ NPs on the surface of g-C_3N_4, the average lifetime were significantly increased, corresponding to 1.98, 2.21 and 1.70 ns, respectively. $Co(OH)_2$ NPs loading remarkably reduced the recombination of carrier and prolonged the lifetime of photogenerated charges. [57,58]

To study the structure and morphology of $Co(OH)_2/C_3N_4$ catalyst, transmission electron microscopy (TEM) was tested and the results were shown in Fig. 5. In Fig. 5 A, the catalysts showed the typical morphology and structure of C_3N_4.[51] The corresponding Selective Area Electron Diffraction (SAED) pattern (insert of Fig. 5 A) suggested the C_3N_4 was in amorphous structure. In Fig. 5B, the $Co(OH)_2$ nanoparticles were uniformly distributed on the surface of C_3N_4. The diameters of those $Co(OH)_2$ nanoparticles were in 2-4 nm. The high-resolution TEM (HRTEM) of $Co(OH)_2/C_3N_4$ catalyst was shown in Fig. 5C. The lattice spacing of 0.24nm could be assigned to the (101) facet of $Co(OH)_2$ and the lattice spacing of 0.27nm could be assigned to the (100) facet of $Co(OH)_2$. In addition, the lattice spacing of 0.34nm was detected, which was due to the dense interlayer-stacking (002) peak of aromatic segment. Fig. 5D clearly showed that the distribution of Co, C, N and O elements were relatively homogeneous in $Co(OH)_2/C_3N_4$ catalyst, which also proved that the $Co(OH)_2$ nanoparticles were uniformly dispersed on the surface of C_3N_4. The energy dispersive X-ray (EDX) measurement also confirmed the co-existence of Co, C, N and O elements in $Co(OH)_2/C_3N_4$ (Fig. 5E). In order to clarify the size distribution of $Co(OH)_2$ nanoparticles, a statistics about 300 nanoparticles was made and the result was shown in the Fig. 5F. The results showed that the size was in the range of 1.5-4.5 nm and the maximum distribution of $Co(OH)_2$ nanoparticles in 3 nm was about 41.7%.

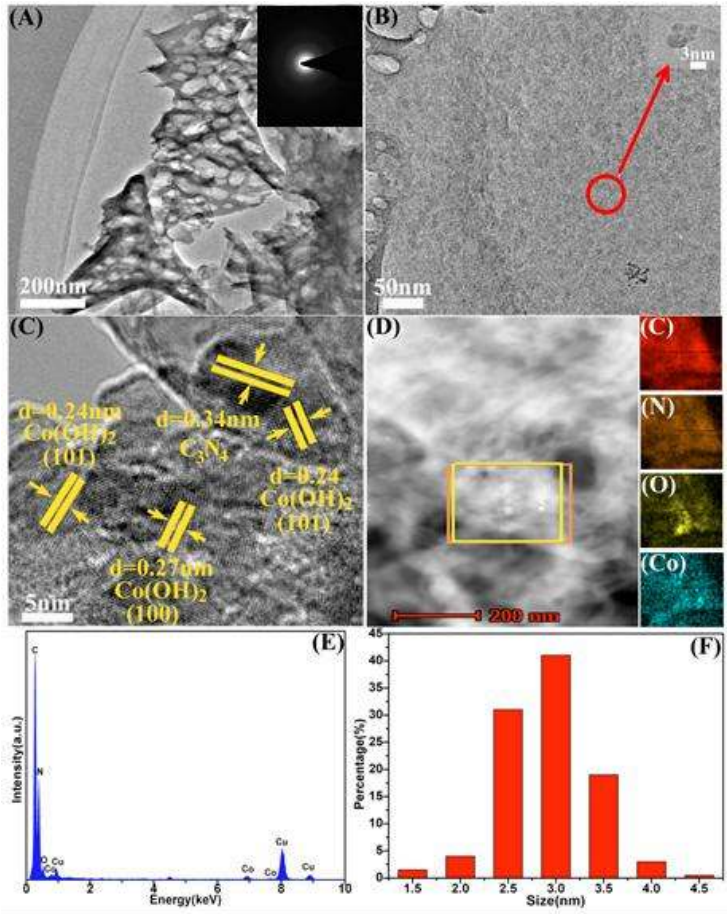

Fig. 5 Transmission electron microscopy images of $Co(OH)_2/C_3N_4$ photocatalyst (A)(B); HRTEM images of $Co(OH)_2/C_3N_4$ photocatalyst (C); HAADF-STEM (high-angle annular dark field scanning transmission electron microscopy) image and elemental mapping images of $Co(OH)_2/C_3N_4$ photocatalyst (D); EDX spectrum of $Co(OH)_2/C_3N_4$ photocatalyst (E) and the distribution of particle size (F).

The time courses of hydrogen evolution in 10% (v/v) TEOA aqueous solution under visible light irradiation ($\lambda \geq 420$ nm) conditions were shown in Fig 6. There was a trace amount of hydrogen evolved over $Co(OH)_2/C_3N_4$ catalyst without ER sensitization, due to the C_3N_4 weak response to visible light. The rate of hydrogen evolved over $Co(OH)_2/C_3N_4$ catalyst was effectively enhanced with the EY or RB sensitization. 259.5 and 184.2 μmol of hydrogen were evolved over $Co(OH)_2/C_3N_4$ catalyst with the ER addition in 3 hours, respectively. This result confirmed that the ER molecular could absorb the visible light to generate electrons and the charges

further transferred to C_3N_4 for HER reaction. After co-sensitization with ER, the rate of hydrogen evolved over $Co(OH)_2/C_3N_4$ catalyst was further enhanced. About 431.9 μmol of hydrogen evolved over $Co(OH)_2/C_3N_4$ catalyst in 3 hours. It was partially resulted from the broadened absorption range of visible light by co-sensitized dyes. Without the C_3N_4, the suspension dispersion showed low activity for hydrogen evolution. Only 101.3 and 139.9 μmol of hydrogen were evolved with ER dyes. This results implied that the g-C_3N_4 not only provided a large area and nanoporous structure for the confined growth of $Co(OH)_2$, but also greatly facilitated ER molecules assembly on its surface, further promoting the activity *via* improved light harvesting. However, no hydrogen was detected in the EY/g-C_3N_4, RB/g-C_3N_4 and EY-RB/g-C_3N_4 system, due to the absence of active sites for hydrogen evolution and oxygen evolution on the surface of g-C_3N_4. This result indicated $Co(OH)_2$ NPs on the surface of g-C_3N_4 provided the active sites for HER. As a co-catalyst, the $Co(OH)_2$ NPs could efficiently promote surface kinetics of g-C_3N_4.

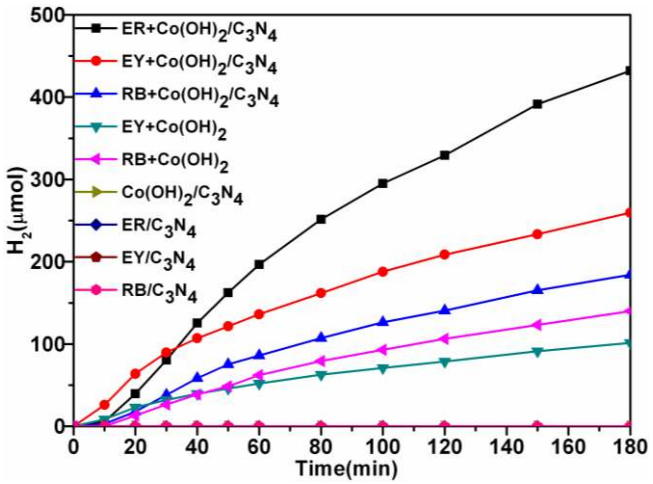

Fig. 6 The time courses of hydrogen evolution catalyzed by $Co(OH)_2/C_3N_4$ with EY and/or RB sensitization in 10% TEOA aqueous solution at pH 9 under visible light irradiation ($\lambda \geq 420$ nm) conditions (100 mW/cm^2).

The UV-vis absorption measurement was carried out to study the response range for visible light. As shown in Figure 7, the absorption edge of C_3N_4 was at about 453 nm (2.74 eV), showing its limited absorption edge in the visible region, which led to the low HER activity. For the EY dye, the light response range is from 440 to 550 nm and

the maximum absorption wavelength is at 518 nm. However, the light response range of RB dye is from 455 to 600 nm and the maximum absorption wavelength is at 548 nm. Interestingly, after the co-sensitization by ER, the absorption range of $Co(OH)_2/C_3N_4$ catalyst was greatly extended from 400 nm toward 600 nm, indicating that the EY sensitization was effective for extending the absorption of C_3N_4 catalyst. This will greatly enhance the light harvesting capability of catalyst for visible light, especially for longer wavelengths among the solar spectrum for efficient HER reaction.

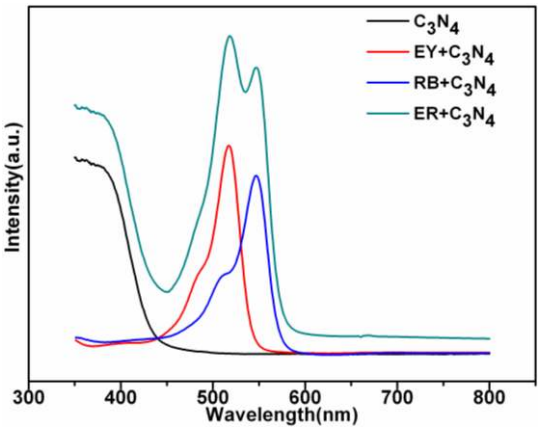

Fig. 7 The UV-vis absorption spectra of $Co(OH)_2/C_3N_4$ photocatalyst with EY and/or RB sensitization.

In order to clearly reveal the extended photo-response and enhanced photocatalytic HER activity of $Co(OH)_2/C_3N_4$ catalyst in longer wavelength visible regions, the wavelength dependence of photocatalytic HER over sensitized photocatalyst was investigated in the range of 430~600 nm using various bandpass filters (λ= 430, 460, 490, 520, and 550 nm). Figure 8 showed the AQEs of hydrogen evolution as a function of the incident light wavelength. The highest AQE reached 33.0% at 430 nm, which was shorter than the wavelength of the highest absorption of EY (518 nm) and RB (548nm) in the visible light range, due to the higher energy of photons[33]. Subsequently, the AQE decreased with increasing wavelengths. The absorption of C3N4 decrease significantly from 420 to 500nm. Therefore, the hydrogen production decreased with wavelength increase from 420 to 490 nm, which corresponds to the

UV-vis absorption. However, the AQE increased at 530 nm and 560 nm due to the strong absorption wavelength of the EY (518 nm) and RB (548nm) dye, corresponding to AQEs of 29.6 and 27.3%, respectively. These results indicated that the HER activities correspond basically with the major absorption wavelength of the ER, which revealed that the light absorption property of the photosensitizer governed the HER rate.

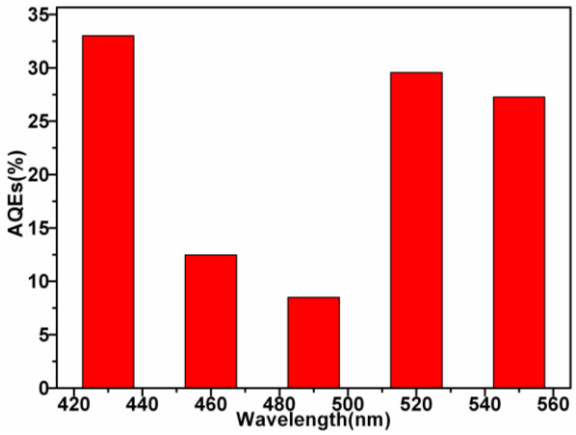

Fig. 8 The AQEs of C_3N_4 $Co(OH)_2/C_3N_4$ photocatalyst with ER co-sensitization under a wide range of visible light irradiation (100 mW/cm^2) at pH 9 from 400 to 600 nm.

The activities of hydrogen evolution at different pHs (5, 7, 9, 11 and 13) were investigated to optimize the reaction condition and the results were shown in Fig. 9. The highest activity of hydrogen evolution was achieved at pH 9. About 431.9 μmol of hydrogen was evolved over $Co(OH)_2/C_3N_4$ catalyst in ER co-sensitized suspension dispersion. With the increase of acidity, the decrease of hydrogen evolution activity might be due to the instability of $Co(OH)_2$ and the protonation of TEOA in acidic solution.[55] That protonation process would impact the electron-donating properties of TEOA and the absorption performance of ER in the visible light region. However, with the increase of alkaline, the activity of hydrogen evolution also decreased. No hydrogen was detected at pH 13. It resulted from the decrease of proton concentration and the fact that hydrogen evolution became more thermodynamically unfavorable with increasing pH values.[56-58] The effect of Co loading on the surface of C_3N_4 catalyst was also carried out to optimize the reaction condition and the results were

shown in Fig. 10. The activity of hydrogen evolution increased with the Co loading increase. When the Co loading was 30%, the highest activity of hydrogen evolution was achieved, corresponding to 432.0 μmol in 3 hours. Further increase of the Co loading, the activity of hydrogen evolution gradually decreased. The excess Co species might result in the agglomeration of $Co(OH)_2$ NPs, which affected its dispersion on the surface of g-C_3N_4. The formed large size $Co(OH)_2$ might also expose less active site for HER. In addition, the excess $Co(OH)_2$ NPs might provide more sites for the charge carrier recombination and reverse reaction. The excess $Co(OH)_2$ NPs loading on the surface of g-C_3N_4 might affect its light absorption performance by scattering and reflection. In addition, the ratio effect of EY to RB on hydrogen evolution was also carried out to optimize the reaction condition and the results were shown in Fig. 11. The highest activity of hydrogen evolution was achieved when the ratio of ER was 1:1, corresponding to 432.0 μmol in 3 hours. When the ratios of ER were 3:1, 2:1, 1:2 and 1:3, only 333.3, 345.4, 324.4 and 251.5 μmol of hydrogen evolved over $Co(OH)_2/C_3N_4$ catalyst in 3 hours, respectively.

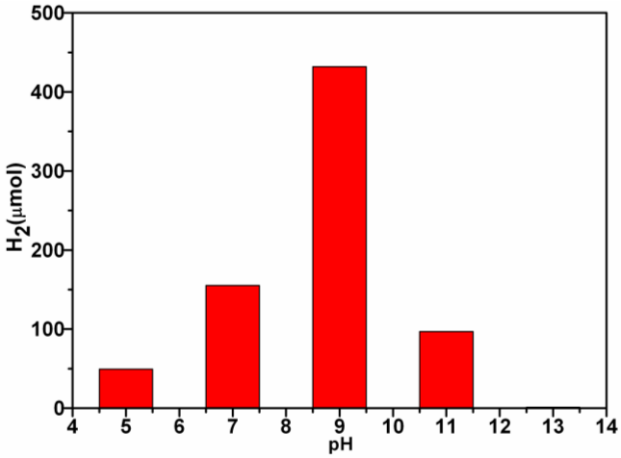

Fig. 9 The effect of pH on photocatalytic activity of $Co(OH)_2/C_3N_4$ photocatalyst with ER co-sensitization for hydrogen evolution under visible light irradiation ($\lambda \geqslant 420$ nm, 100 mW/cm^2) in 10% TEOA aqueous solution at pH 9. (The reaction time was 3 h and light intensity was 100mW/cm^2)

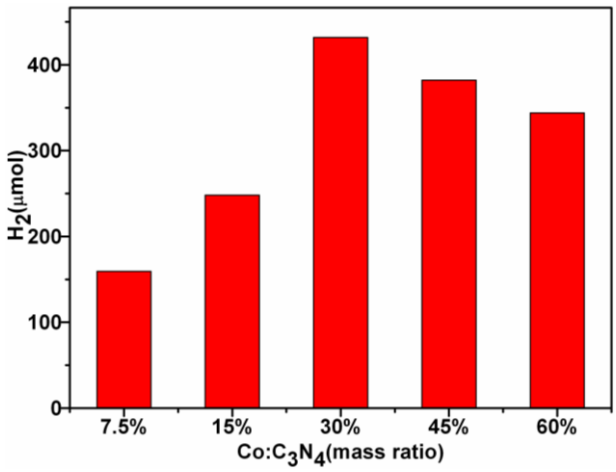

Fig. 10 The effect of the amount of Co on the activity of hydrogen evolution over g-C_3N_4 photocatalyst under visible light irradiation (λ≥420 nm)in 10% TEOA aqueous solution at pH 9. (The reaction time was 3 h and light intensity was 100mW/cm^2)

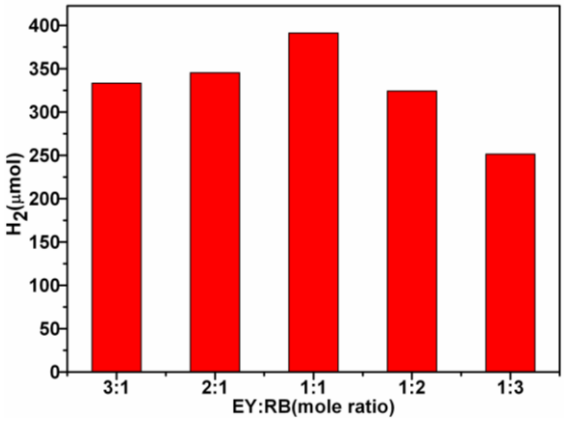

Fig. 11 The effect of the molar ratios of ER dyes on the activity of hydrogen evolution over $Co(OH)_2/C_3N_4$ photocatalyst under visible light irradiation (λ≥420 nm) in 10% TEOA aqueous solution at pH 9. (The reaction time was 3 h and light intensity was 100mW/cm^2)

Photoelectrochemical experiments were performed to study the photoinduced electron transfer processes. As shown in Figure 12, the response to visible light could be seen during on−off cycles of visible light irradiation, while the $Co(OH)_2/C_3N_4$/ITO electrode produced a low photocurrent. The observed unbiased transient photocurrent with the dye sensitized $Co(OH)_2/C_3N_4$/ITO electrode was promoted under similar

experimental conditions. The maximum photocurrents were 24.3 and 18.9 μA/cm^2 after sensitized by ER, respectively. Co-sensitized $Co(OH)_2/C_3N_4$/ITO electrode by ER showed more positive photocurrent, corresponding to 41.3 μA/cm^2, suggesting electron injection from the photoexcited EY to the C_3N_4.[59] This result further highlights the importance of the co-sensitization effect of ER and excited state electron transfer in generating a photoelectrochemical effect. However, the observed photocurrent densities of sensitized $Co(OH)_2/C_3N_4$/ITO electrodes were still low in the present experiments. Although the excited state of ER can be quenched by C_3N_4 through electron transfer, a fast recombination of charge carriers will probably result in a very low net generation of photocurrent. In addition, the electrochemical hydrogen evolution activities of C_3N_4 and $Co(OH)_2/C_3N_4$ deposited on ITO glass were also investigated using the linear sweep voltammetry (LSV) technique. As shown in Fig. 13, the cathodic current of bare ITO electrode belonged to the reduction of water to hydrogen was low with the increase of the applied potential.[60] The cathodic currents of C_3N_4/ITO electrode only had a relative enhancement. However, the $Co(OH)_2/C_3N_4$/ITO electrode exhibited a significant improvement beyond -0.4 V, which proved that $Co(OH)_2$ NPs were remarkable active sites which could efficiently catalyze the reduction of water to hydrogen. Moreover, the $Co(OH)_2$ NPs modified the g-C_3N_4 showed a low onset potential (0.26V) as shown in the insert of Fig. 13.

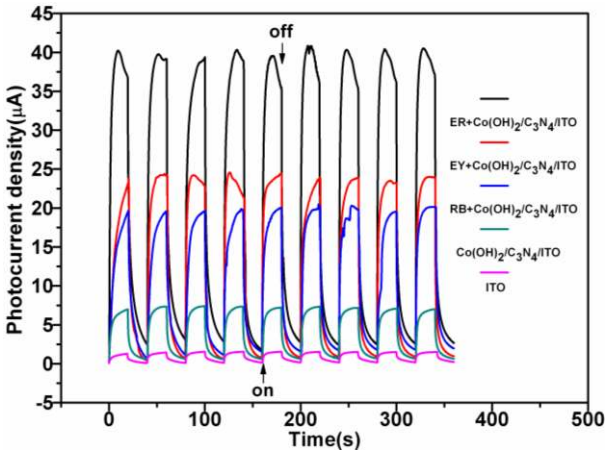

Fig. 12 Transient photocurrent time profiles of $Co(OH)_2/C_3N_4$ photocatalyst with EY and/or RB sensitization on ITO glass in mixed solution of 10% (v/v) TEOA and 0.1 M Na_2SO_4 at pH 9 under visible light irradiation (λ≥420 nm, 100mW/cm^2).

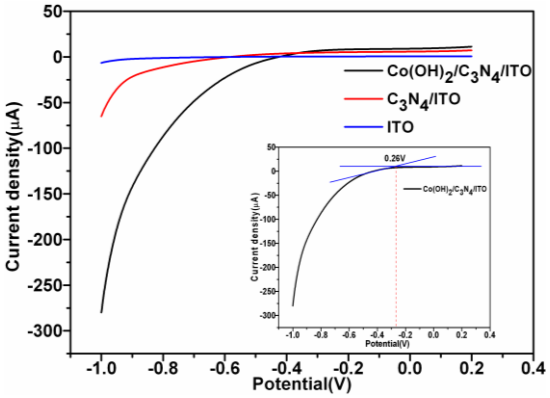

Fig. 13 LSV curves of g-C_3N_4 and $Co(OH)_2/C_3N_4$ photocatalysts coated on ITO glass in mixed solution of 10% (v/v) TEOA and 0.1 M Na_2SO_4 aqueous solution at pH 9.

The stabilities of hydrogen evolution over $Co(OH)_2/C_3N_4$ catalyst co-sensitized by ER were tested under visible light irradiation ($\lambda \geq 420$nm). As shown in Fig. 14, the catalysts were stable during 900 min reaction. After each run, the catalysts were collected by centrifuging from the reaction mixture and redispersed in the fresh TEOA aqueous solution. The rates of hydrogen evolution remained almost no change in every run. These results indicate that the $Co(OH)_2/C_3N_4$ catalyst is significantly stable during the photocatalytic HER processes.

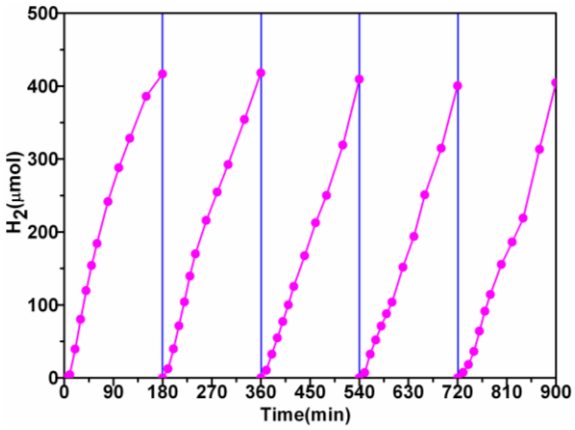

Fig.14 The stabilities of hydrogen evolution over $Co(OH)_2/C_3N_4$ photocatalysts under visible light irradiation ($\lambda \geq 420$ nm, 100mW/cm^2) at pH 9. The reaction was continued for 900 min. After every run, the catalysts were collected by centrifuging from the reaction mixture and redistributed in the fresh 10% TEOA aqueous solution with 17 mg EY and 25 mg RB dyes and then evacuated.

The reaction process of photocatalysis hydrogen evolution in the co-sensitized $Co(OH)_2/C_3N_4$ catalyst system can be explained in terms of Scheme 2. The ER dye molecules absorb visible light photon to form singlet excited state EY^{1*} and RB^{1*} under visible light irradiation, and then produces the lowest-lying triplet excited state EY^{3*} and RB^{3*} *via* an efficient intersystem crossing. EY^{3*} and RB^{3*} can be reductively quenched by TEOA and produce $EY^{-\bullet}$, $RB^{-\bullet}$ and oxidative donor ($TEOA^+$).[9, 61] The e^- of $EY^{-\bullet}$ and $RB^{-\bullet}$ species is transferred to C_3N_4 by the noncovalent π-π stacking interaction due to its electron transport characteristics, which leads to spatially separation of photogenerated charges.[62] The accumulated electrons on the C_3N_4 will transfer to $Co(OH)_2$ nanoparticles. Subsequently, those electrons improve the reduction of H^+ to form hydrogen. In addition, the semiconductor C_3N_4 can also absorb part of visible light to generate carrier pair. Those electrons are used to reduce the H^+.

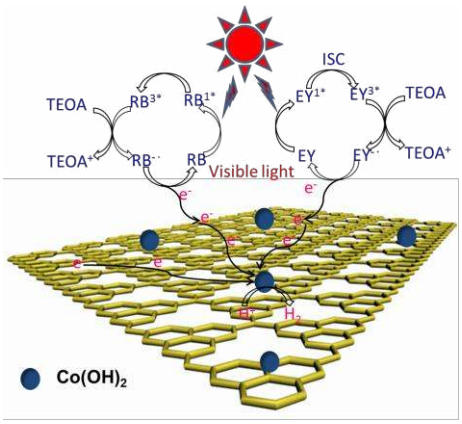

Scheme 2 The proposed reaction mechanism for visible-light-driven water splitting by $Co(OH)_2/C_3N_4$ photocatalyst with ER co-sensitization.

Conclusion

Non-noble metal cobalt hydroxide NPs modified the g-C_3N_4 by in-situ chemical deposition methods exhibited a low onset potential (0.26V) and high photocatalytic activity for HER after co-sensitized by ER dyes. The g-C_3N_4 not only provided a large area and nanoporous structure for the confined growth of $Co(OH)_2$, but also greatly facilitated ER molecules assembly on its surface, which could further promote the HER activity by improving light harvesting. In this process, the ER, owning strong

absorption ability for visible light, as co-sensitizer could expand the light absorption rang of $Co(OH)_2/C_3N_4$ from UV light to 600 nm. The amount of hydrogen evolution over $Co(OH)_2/C_3N_4$ co-sensitized by ER dyes was about 431.9 μmol in 3 hours under visible light irradiation. In addition, this sensitization photocatalyst also showed rather stable photocatalytic activity for HER under visible light irradiation. The apparent quantum efficiency (AQE) of 29.6 and 27.3% were achieved at 530 nm and 560 nm, respectively, due to the strong absorption wavelength of the EY (518 nm) and RB (548nm) dye. These results indicate that the $Co(OH)_2$ NPs modified g-C_3N_4 renders a stable and high efficient activity for hydrogen evolution after co-sensitizing by ER.

AUTHOR INFORMATION

Corresponding Author

*E-mail: gxlu@lzb.ac.cn. Tel.: +86-931-4968 178.

ACKNOWLEDGMENT

This work is supported by the NSF of China (grant no. 21173242 and 21433007), respectively.

References

(1) Y. Zheng, L. H. Lin, B. Wang, X. C. Wang, Angew. Chem. Int. Ed. 54 (2015) 12868-12884.

(2) X. B. Chen, S. H. Shen, L. J. Guo, S. S. Mao, Chem. Rev. 110 (2010) 6503−6570.

(3) L. Ma, X. Kang, S. Hu, F. Wang, J. Mol. Catal. (China) 29 (2015) 359-368.

(4) A. Iwase, Y. H. Ng, Y. Ishiguro, A. Kudo, R. Amal, J. Am. Chem. Soc. 133 (2011) 11054−11057.

(5) J. S. Zhang, Y. Chen, X. C. Wang, Energy Environ. Sci. 8 (2015) 3092-3108.

(6) X. H. Zhang, T. Y. Peng, L. J. Yu, R. J. Li, Q. Q. Li, Z. Li, ACS Catal. 5 (2015) 504−510.

(7) Z. Li, C. Kong, G. X. Lu, J. Phys. Chem. C 120 (2016) 56-63.

(8) X. C. Wang, K. Maeda, A. Thomas, K. Takanabe, G. Xin, J. M. Carlsson, K. Domen, M. Antonietti, Nat. Mater. 8 (2009) 76−80.

(9) S. X. Min, G. X. Lu, J. Phys. Chem. C 116 (2012) 19644-19652.

(10) X. F. Chen, J. S. Zhang, X. Z. Fu, M. Antonietti, X. C. Wang, J. Am. Chem. Soc. 131 (2009) 11658−11659.

(11) Z. X. Ding, X. F. Chen, M. Antonietti, X. C. Wang, ChemSusChem 4 (2011) 274−281.

(12) X. C. Wang, X. F. Chen, A. Thomas, X. Z. Fu, M. Antonietti, Adv. Mater. 21 (2009) 1609−1612.

(13) B. Yue, Q. Y. Li, H. Iwai, T. Kako, J. H. Ye, Sci. Technol. Adv. Mater. 12 (2011) 1−7.

(14) G. Liu, P. Niu, C. H. Sun, S. C. Smith, Z. G. Chen, G. Q. Lu, H. M. Cheng, J. Am. Chem. Soc.132 (2010) 11642−11648.

(15) J. S. Zhang, J. H. Sun, K. Maeda, K. Domen, P. Liu, M. Antonietti, X. Z. Fu, X. C. Wang, Energy Environ. Sci 4 (2011) 675−678.

(16) S. C. Yan, Z. S. Li, Z. G. Zou, Langmuir 26 (2010) 3894−3901.

(17) Y. Wang, Y. Di, M. Antonietti, H. R. Li, X. F. Chen, X. C. Wang, Chem. Mater. 22 (2010) 5119−5121.

(18) Y. J. Zhang, T. Mori, J. H. Ye, M. Antonietti, J. Am. Chem. Soc. 132 (2010) 6294–6295.

(19) J. S. Zhang, X. F. Chen, K. Takanabe, K. Maeda, K. Domen, J. D. Epping, X. Z. Fu, M. Antonietti, X. C. Wang, Angew. Chem. Int. Ed. 49 (2010) 441–444.

(20) Y. J. Wang, R. Shi, J. Lin, Y. F. Zhu, Energy Environ. Sci. 4 (2011) 2922–2929.

(21) S. C. Yan, S. B. Lv, Z. S. Li, Z. G. Zou, Dalton Trans. 39 (2010) 1488–1491.

(22) H. J. Yan, Y. Huang, Chem. Commun. 47 (2011) 4168–4170.

(23) L. Jia, D. H. Wang, Y. X. Huang, A. W. Xu, H. Q. Yu, J. Phys. Chem. C 115 (2011) 11466–11473.

(24) Q. J. Xiang, J. G. Yu, M. Jaroniec, J. Phys. Chem. C 115 (2011) 7355–7363.

(25) X. C. Wang, K. Maeda, X. F. Chen, K. Takanabe, K. Domen, Y. D. Hou, X. Z. Fu, M. Antonietti, J. Am. Chem. Soc. 131 (2009) 1680–1681.

(26) X. F. Chen, Y. S. Jun, K. Takanabe, K. Maeda, K. Domen, X. Z. Fu, M. Antonietti, X. C. Wang, Chem. Mater. 21 (2009) 4093–4095.

(27) F. Z. Su, S. C. Mathew, G. Lipner, X. Z. Fu, M. Antonietti, S. Blechert, X. C. Wang, J. Am. Chem. Soc. 132 (2010) 16299–16301.

(28) K. Kwon, Y. J. Sa, J. Y. Cheon, S. H. Joo, Langmuir 28 (2012) 991–996.

(29) H. J. Yan, Chem. Commun. 48 (2012) 3430–3432.

(30) J. Burschka, N. Pellet, S. Moon, R. Humphry-Baker, P. Gao, M. Nazeeruddin, M Graetzel, Nature 499 (2013) 316–319.

(31) S. Peng, M. Ding, T. Yi, Y. Li, J. Mol. Catal. (China) 28 (2014) 466-473.

(32) M. G. Walter, E. L. Warren, J. R. McKone, S. W. Boettcher, Q. Mi, E. A. Santori, et al. Chem Rev. 110 (2010) 6446-6473.

(33) H. Yan, J. Yang, G. Ma, G. Wu, X. Zong, Z. Lei, et al. J. Catal. 266 (2009) 165-168.

(34) A. Gasparotto, D. Barreca, D. Bekermann, A. Devi, R. A. Fischer, P. Fornasiero, et al. J. Am. Chem. Soc. 133 (2011) 19362-19365.

(35) M. W. Kanan, D. G. Nocera, Science 321 (2008) 1072-1075.

(36) P. Du, J. Schneider, G. Luo, W. W. Brennessel, R. Eisenberg, Inorg. Chem. 48 (2009) 4952-4962.

(37) G. G. Zhang, S. H. Zang, X. C. Wang, ACS Catal. 5 (2015) 941−947.

(38) O. Pantani, S. Naskar, R. Guillot, P. Millet, E. A. Mallart, A. Aukauloo, Angew. Chem. Int. Ed. 47 (2008) 9948-9950.

(39) G. G. Zhang, C. J. Huang and X. C. Wang, Small 11 (2015) 1215-1221.

(40) G. G. Zhang, S. H. Zang, Z. A. Lan, C. J. Huang, G. S. Li, X. C. Wang, J. Mater. Chem. A 3 (2015) 17946-17950.

(41) V. Artero, M. Chavarot-Kerlidou, M. Fontecave, Angew. Chem. Int. Ed. 50 (2011) 7238-7266.

(42) S. Yu, Z. J. Li, X. B. Fan, J. X. Li, F. Zhan, X. B. Li, Y. Tao, C. H. Tung, L. Z. Wu, ChemSusChem 8 (2015) 642-649.

(43) Z. L. Wang, G. J. Liu, C. M. Ding, Z. Chen, F. X. Zhang, J. Y. Shi, C. Li, J. Phys. Chem. C 119 (2015) 19607-19612.

(44) H. F. Dang, X. F. Dong, Y. C. Dong, H. B. Fan, Y. F. Qiu, Mater Lett 138 (2015) 56-59.

(45) H. Wender, R. V. Gonçalves, C. S. B. Dias, M. J. M. Zapata, L. F. Zagonel, E. C. Mendonça, S. R. Teixeira, F. Garcia, Nanoscale 5 (2013) 9310-9316.

(46) J. R. Ran, J. Zhang, J. G. Yu, S. Z. Qiao, ChemSusChem 7 (2014) 3426-3434.

(47) M. J. Bojdys, J. O. Müller, M. Antonietti, A. Thomas, Chem. Eur. J. 14 (2008) 8177-8182.

(48) D. X. Shi, X. F. Zhang, L. Yuan, Y. S. Gu, Y. P. Zhang, Z. J. Duan, X. R. Chang, Z. Z. Tian, N. X. Chen, Appl. Surf. Sci. 148 (1999) 50-55.

(49) D. L. Yu, F. R. Xiao, T. S. Wang, Y. J. Tian, J. L. He, D. C. Li, W. K. Wang, J. Mater. Sci. Lett. 19 (2000) 553-556.

(50) V. N. Khabashesku, J. L. Zimmerman, J. L. Margrave, Chem. Mater. 12 (2000) 3264-3270.

(51) J. Liu, Y. Liu, N. Y. Liu, Y. Z. Han, X. Zhang, H. Huang, Y. Lifshitz, S. T. Lee, J. Zhong, Z. H. Kang, Science 347 (2015) 970-974.

(52) T. Komatsu, T. Nakamura, J. Mater. Chem. 11 (2001) 474-478.

(53) Q. X. Guo, Y. Xie, X. J. Wang, S. Y. Zhang, T. Hou, S. H. Lv, Chem. Commun. 1 (2004) 26-27.

(54) A. Thomas, A. Fischer, F. Goettmann, M. Antonietti, J. O. Müller, R. Schlögl, J. M. Carlsson, J. Mater. Chem. 18 (2008) 4893-4908.

(55) T. Shimidzu, T. Iyoda, Y. Koide, J. Am. Chem. Soc. 107 (1985) 35-41.

(56) K. Kalyanasundaram, J. Kiwi, M. Graetzel, Helv. Chim. Acta. 61 (1978) 2720−2730.

(57) Z. Li, Q. S. Wang, C. Kong, Y. Q. Wu, Y. X. Li, G. X. Lu, J. Phys. Chem. C 119 (2015) 13561-13568.

(58) Z. Li, C. Kong, G. X. Lu, Int. J. Hydrogen Energ. 40 (2015) 9061-9068.

(59) A. Wojcik, P. V. Kamat, ACS Nano 4 (2010) 6697−6706.

(60) X. Zong, G. P. Wu, H. J. Yan, G. J. Ma, J. Y. Shi, F. Y. Wen, et al. J. Phys. Chem. C 114 (2010) 1963-1968.

(61) K. Maeda, M. Eguchi, S. H. A. Lee, W. J. Youngblood, H. Hata, T. E. Mallouk, J. Phys. Chem. C 113 (2009) 7962-7969.

(62) S. X. Min, G. X. Lu, J. Phys. Chem. C116 (2012) 25415-25424.